Micro-environmental control of cell migration – myosin IIA is required for efficient migration in fibrillar environments through control of cell adhesion dynamics

Andrew D. Doyle[1,*], Matthew L. Kutys[1], Mary Anne Conti[2], Kazue Matsumoto[1], Robert S. Adelstein[2] and Kenneth M. Yamada[1,*]

[1]Laboratory of Cell and Developmental Biology, Cell Biology Section, National Institute of Dental and Craniofacial Research; [2]Laboratory of Molecular Cardiology, National Heart, Lung and Blood Institute, National Institutes of Health, Bethesda, MD 20892, USA

*Author for correspondence (adoyle@mail.nih.gov; kyamada@dir.nidcr.nih.gov)

Accepted 17 December 2011
Journal of Cell Science 125, 2244–2256

doi: 10.1242/jcs.098806

Summary

Recent evidence suggests that organization of the extracellular matrix (ECM) into aligned fibrils or fibril-like ECM topographies promotes rapid migration in fibroblasts. However, the mechanisms of cell migration that are altered by these changes in micro-environmental topography remain unknown. Here, using 1D fibrillar migration as a model system for oriented fibrillar 3D matrices, we find that fibroblast leading-edge dynamics are enhanced by 1D fibrillar micropatterns and demonstrate a dependence on the spatial positioning of cell adhesions. Although 1D, 2D and 3D matrix adhesions have similar assembly kinetics, both 1D and 3D adhesions are stabilized for prolonged periods, whereas both paxillin and vinculin show slower turnover rates in 1D adhesions. Moreover, actin in 1D adhesions undergoes slower retrograde flow than the actin that is present in 2D lamellipodia. These data suggest an increase in mechanical coupling between adhesions and protrusive machinery. Experimental reduction of contractility resulted in the loss of 1D adhesion structure and stability, with scattered small and unstable adhesions, and an uncoupling of adhesion protein-integrin stability. Genetic ablation of myosin IIA (MIIA) or myosin IIB (MIIB) isoforms revealed that MIIA is required for efficient migration in restricted environments as well as adhesion maturation, whereas MIIB helps to stabilize adhesions beneath the cell body. These data suggest that restricted cell environments, such as 1D patterns, require cellular contraction through MIIA to enhance adhesion stability and coupling to integrins behind the leading edge. This increase in mechanical coupling allows for greater leading-edge protrusion and rapid cell migration.

Key words: Adhesions, Contractility, Fibrillar, Migration

Introduction

Cell migration is a multifaceted process requiring the coordinated interactions of hundreds of proteins, the cumulative actions of which can be classified into four distinct components: (1) protrusion of the leading edge; (2) adhesion to the surrounding extracellular matrix (ECM); (3) translocation of the cell body and (4) retraction of the trailing edge (Ridley et al., 2003). Regulation of cell migration involves not only internal signaling events, but also external guidance cues originating from the extracellular micro-environment. Soluble signals, such as growth factors and chemoattractants, can promote directional migration through the activation of internal signaling cascades, known as outside-in signalling (Petrie et al., 2009). However, physical cues, such as ECM plasticity and dimensionality, can dictate the mode of cell migration, migration rates and directionality, and activation of mechanotransduction pathways (Friedl and Wolf, 2010).

Recent evidence indicates that cell shape and ECM topography regulate migratory phenotypes. Cancer cells are known to manipulate their environments by aligning collagen bundles in mammary tumors (Provenzano and Keely, 2009), and they subsequently migrate efficiently along ECM fibrils. We have previously shown that ECM fibrils can be mimicked by linear, 1D micropatterns (Doyle et al., 2009). By altering ECM topography and limiting cells to a single 1D fibril-like matrix, fibroblasts demonstrate enhanced migration that is similar to cell migration on fibrils of an oriented 3D cell-derived matrix (CDM). In both 1D and 3D settings, the migratory and cytoskeletal phenotypes were different from those observed on 2D substrates. To better understand how external environmental factors, such as ECM topography, play a role in regulating cell migration, we addressed the following question: how does linear 1D topography increase the efficiency of fibroblast migration?

Each part of the migration process is tightly regulated internally, and is influenced by numerous external signaling cascades and events. For example, actin polymerization at the leading edge is dependent on the critical concentration of free actin monomers (Kiuchi et al., 2007) that is governed by the activities of profilin, Arp2/3, mDia and other formins, several GTPases, Mena/VASP family members, Akt and PI3-kinase activity, as well as many other proteins (Ridley, 2011). The act of

protrusion involves actin polymerization to exert force against the plasma membrane. These protrusive forces emanate from the lamella that are attached to the ECM, in most cases resulting in the formation of either broad lamellipodia or narrow filopodia that probe the surrounding environment before attachment to the ECM. In order for protrusive forces to distend the plasma membrane, actin must polymerize at a rate faster than the rate of actin retrograde flow, which is dependent on myosin II motor proteins pulling actin filaments towards the cell center (Parsons et al., 2010). The correct balance of these pushing and pulling forces within cells acts to drive leading-edge dynamics and forwards cell migration. However, little is known about whether external physical factors can regulate leading-edge dynamics.

The formation of adhesions that integrate the connection between the underlying extracellular matrix and the actin cytoskeleton is also regulated by numerous signals, including protein phosphorylation and protein recruitment, types of integrins involved, and the levels of actomyosin contractility. As with cellular protrusion, myosin II contraction plays a prominent role in regulating focal adhesions (Vicente-Manzanares et al., 2007). Recent evidence indicates that contractile force controls not only the formation and size of focal adhesions, but also the relative lifetime or stability of these physical linkages to the ECM (Gupton and Waterman-Storer, 2006). A loss of contractile force leads to the disassembly of focal adhesions (FAs), demonstrating their dependence on cellular contraction (Vicente-Manzanares et al., 2007; Pasapera et al., 2010). FAs provide a physical link between the ECM and the actin cytoskeleton within the lamella by a postulated molecular clutch mechanism that locally reduces the retrograde flow of actin. The clutch is thought to integrate rapid actin retrograde flow with the relatively stable (low or no flow) integrin–ECM linkage (Hu et al., 2007). This concept suggests that the relative stability of adhesions within the lamella regulates actin within the leading edge. Because myosin II contractility can influence both protrusion and adhesion, we have investigated why myosin II is required for efficient 1D and 3D migration (Doyle et al., 2009), but is not required for maintaining velocity in 2D migration.

To answer these questions, we utilized 1D fibrillar migration as a model system to determine how physical cues from the ECM can regulate the various elements of cell migration. Here, we establish that altering the spatial attributes of the ECM directly affects adhesion dynamics, which in turn regulate protrusion at the leading edge. Specifically, we find that protrusion of the leading edge is enhanced under 1D conditions, and that 1D adhesion complexes and 3D matrix adhesions show enhanced adhesion stability compared with that of FAs that are formed on 2D substrates. Fibroblasts migrating on 1D topographies demonstrated an increased mechanical coupling to the ECM, as shown by reduced turnover rates of paxillin, vinculin and actin, compared with 2D substrates. Treatment of cells on 1D substrates with the myosin II inhibitor blebbistatin substantially inhibited migration and caused dissociation between activated β1 integrin and paxillin, suggesting that actin-based contractile forces are required to more fully engage the molecular clutch necessary for maintaining the efficiency of 1D migration. Knockdown or genetic ablation experiments revealed a requirement for myosin IIA (MIIA, encoded by *MYH9*) during 1D migration even though myosin IIB (MIIB, encoded by *MYH10*) was required for 1D adhesion stabilization. We conclude that cellular contractile forces are required under environmental conditions that would otherwise impede migration, and that cells respond by enhancing their mechanical coupling to the surrounding environment.

Results

ECM topography alters cellular protrusion dynamics and leading-edge efficiency

We previously established that cells migrating on 1D fibril-like structures resemble cells migrating in 3D matrices, but not cells migrating on regular 2D tissue culture substrates, exhibiting a more rapid migration and a dependence on actomyosin contractility that is not observed on 2D surfaces (Doyle et al., 2009). Because the mechanisms of these differences were not clear, we have elucidated how 1D fibrillar substrates promote rapid migration. During forwards movement, the lamellipodium undergoes periodic protrusion–retraction (P–R) cycles associated with cytoskeletal contraction within the lamella at FA sites (Giannone et al., 2007). Because leading edge protrusion on fibrillar patterns is the rate-limiting process during migration and is independent of tail retraction (Doyle et al., 2009), we examined whether P–R cycles depend on topographical cues.

We first quantified protrusive activities of NIH-3T3 fibroblasts during directional cell migration on 2D substrates involving a single major lamellipodium. Kymograph analysis of high-resolution phase-contrast images confirmed a definitive P–R cycle that originates at, and returns to, the lamella–lamellipodial (LP–LA) border at a frequency of 0.65 ± 0.87 min^{-1} (Fig. 1A; Fig. 2D). As previously reported for Chinese hamster ovary (CHO) cells in 2D (Choi et al., 2008), the P–R cycle led to a stepwise progression of the lamella (Fig. 1A, red line). This stepping was associated with the formation of a new FA at each step, as indicated by GFP–paxillin localization (Fig. 2A,B). To compare and contrast 1D and 2D P–R cycles, we calculated protrusion and retraction distances as well as net protrusion (net forwards movement of lamellar). During a single P–R cycle, protrusion and retraction distances on 1D substrates were increased and decreased, respectively, resulting in substantially enhanced rates of net protrusion (Fig. 1C). These cells migrating on a single 1.5–2 μm-wide line also demonstrated nearly twofold increases in P–R cycle frequency, with 2.8-fold increases in protrusion rate (Fig. 2D,E; supplementary material Movie 1). Notably, 1D migration showed smooth forwards LA–LP border progression without the stepwise lamellar advance seen in 2D (Fig. 1B, red line). These alterations resulted in enhanced cell protrusion and increased migration rates in 1D versus 2D settings.

In 2D migration, newly formed adhesions across the entire leading edge are involved in the forwards advance of the lamella (Burnette et al., 2011). Because 1D lines restrict adhesions to a very narrow zone or line, we analyzed the entire lamellipodium of cells on 2D substrates as a single unit (green boxed areas versus the single yellow line in Fig. 2A), by performing kymograph analysis across its entire breadth. By observing GFP–paxillin together with phase-contrast images (using maximal intensity for projection), we found that, in contrast to the stepping motion in standard kymographs (Fig. 2A), this grouped kymograph of the entire leading edge showed a linear advance associated with progressive anchoring of adhesions to the ECM. This linear pattern of advance mimics the linear leading-edge dynamics of cells migrating on a 1D fibrillar pattern. These results suggest that the configuration of adhesions

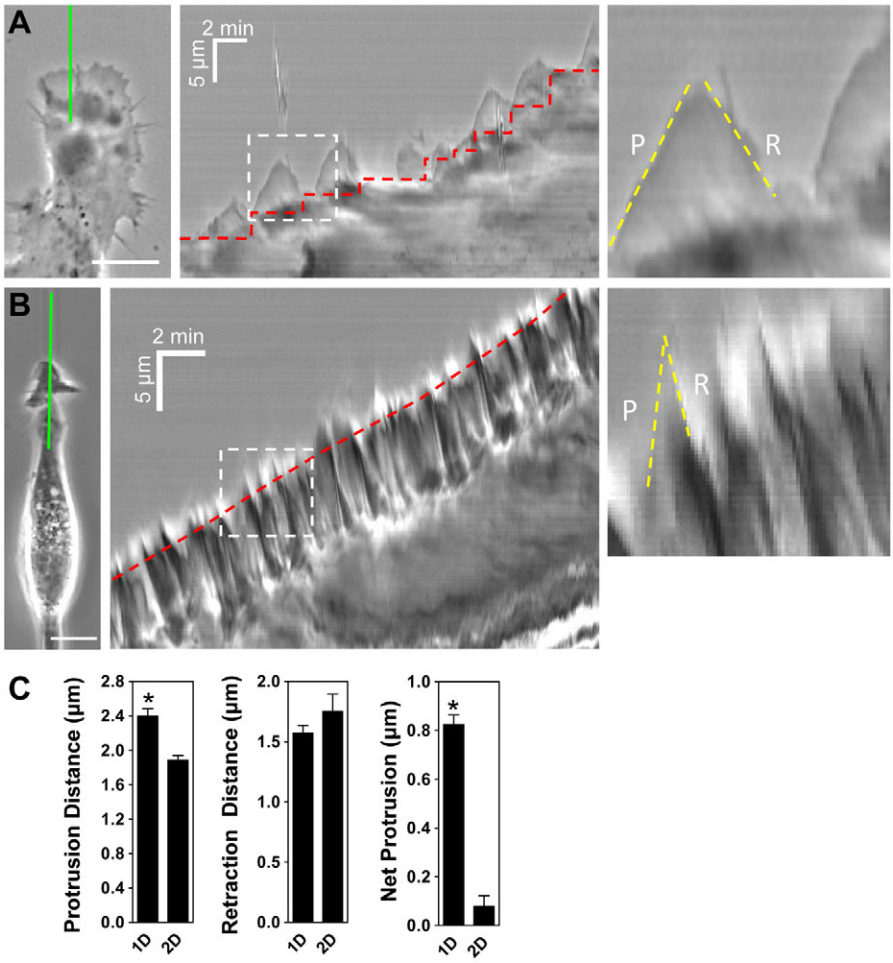

Fig. 1. Comparison of protrusion efficiency. (**A**,**B**) Phase-contrast images of NIH/3T3 fibroblasts migrating on 2D (A) or 1D micropatterned (B) surfaces. Kymograph analysis at the green lines (right panels and insets) shows local protrusion–retraction cycles, with forwards progression of the lamellipodial–lamellar border (red dotted line). Yellow dotted lines indicate protrusion (P) and retraction (R) phases. (**C**) Analyses of protrusion, retraction and net cellular protrusion per cycle between 1D and 2D conditions. Scale bars: 10 µm unless otherwise indicated. *$P<0.05$.

behind the leading edge (a single long adhesion versus multiple FAs that are spread laterally) affects the patterns of protrusion dynamics and lamellar advance.

In order to test the hypothesis that lateral separation into discrete adhesion sites along a broad lamellipodium explains the lower frequency of P–R cycles in 2D directional migration, we generated multiple dotted lines to mimic the spacing between adhesions that is normally associated with 2D surfaces (1.6 µm diameter dots with 3 µm center-on-center spacing across 12 µm-wide lanes (Fig. 2C). P–R cycle analysis revealed that this experimental spatial separation of FAs leads to the predicted reduction in cycle frequency as well as reduced protrusion velocity. Taken together, these data indicate that altering the physical constraints of an ECM can modify the dynamics of P–R cycling at the leading edge and regulate the speed of cell migration. The lateral spacing of adhesions along the lamellipodia–lamella border, thus, determines local P–R cycle frequency.

Adhesion longevity depends on the cellular microenvironment

We previously showed that in cells migrating on 1D fibrillar patterns, vinculin and paxillin were localized along the entire length of a single, long 1D cell adhesion (Doyle et al., 2009). Here, we tested whether ECM topography can alter the kinetics of adhesion formation and stabilization (Fig. 3A,B). As a standard for comparison, total internal reflection fluorescence (TIRF) microscopy of NIH-3T3 fibroblasts stably transfected with GFP– or YFP–paxillin and plated on 2D fibronectin confirmed the formation of both nascent adhesions (NAs) and FAs. NAs were characterized by their small size (~1 µm^2 or smaller) and short lifespan at the leading edge. FAs were larger [generally ≥2 µm^2 and more stable (see below)]. As previously reported (Choi et al., 2008), assembly rates for NAs were substantially faster than for focal adhesions, and they had a short stability-phase (the time point when the adhesion is neither assembling nor disassembling) compared with the more stable FAs.

By contrast, 1D adhesions demonstrated assembly kinetics similar to those of FAs (Fig. 3C,D). In fact, the relatively transient NAs characteristically present within the lamellipodia of cells in 2D were absent in the 1D model; once an adhesion formed, it remained stable, suggesting that all adhesions mature. Although 1D adhesion assembly rates were similar to those of FAs, a striking difference was found in the stability phase. 1D adhesions maintained prolonged stability that was sixfold longer than that of FAs (Fig. 3C,E,F).

Because cells migrating on 1D lines demonstrate many properties similar to cells migrating through a fibrillar 3D CDM, we next determined whether adhesion kinetics for 3D matrix adhesions were similar. To analyze 3D matrix adhesions, fibroblasts expressing GFP–paxillin were allowed to migrate into a 3D CDM labeled with Alexa Fluor 568 dye to visualize the

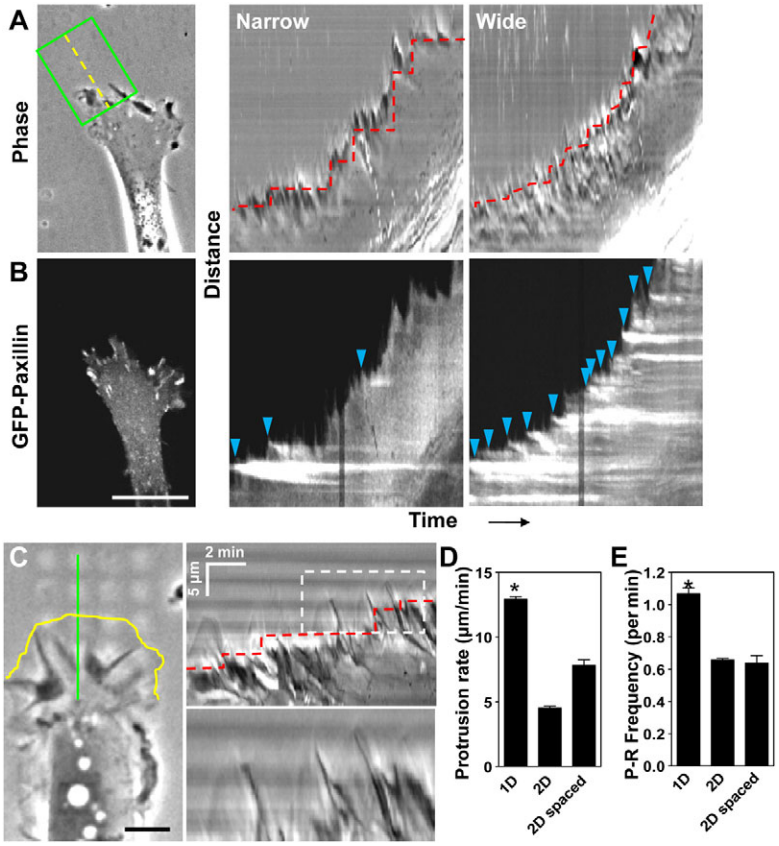

Fig. 2. Lamellar movement in 2D migration is associated with local adhesion formation. (**A**) Phase contrast with narrow (center panel) versus wide (right panel) kymograph analysis of 2D directional migration. The red dotted line indicates the lamellipodial–lamellar border; kymograph analysis is shown at the yellow dotted line. (**B**) GFP–paxillin expression in the same cell as in A. The narrow kymograph (at the yellow dotted line) shows few adhesions (blue arrowheads) whereas the wide kymograph (green box) demonstrates fluid forwards progression with more adhesions. (**C**) Lateral separation of adhesion sites causes a reduction in protrusion rate and P–R cycle frequency. The kymographs (right upper panel and enlarged lower panel) show a reduction in frequency. (**D**) Protrusion rates for 1D, 2D and 2D-spaced micropatterns. (**E**) Differences in P–R frequency per minute between conditions. *$P<0.05$. Scale bars: B, 10 µm and C, 3 µm.

matrix. Adhesions formed primarily along the long axis of matrix fibers. Interestingly, as with 1D adhesions, discernible NAs were not detected. Once cells contacted a matrix fiber, a GFP-positive adhesion formed where the cell actively pulled and displaced the fiber rearward toward the cell center (Fig. 3G,H; supplementary material Movie 2). Adhesion stabilization coincided with the cessation of further fiber displacement, suggesting that a steady-state-force balance was reached between the cell and the ECM fiber. This lengthy stability phase in 3D was similar to 1D, but not to 2D or NAs. Because imaging times often varied, we calculated the percentage of adhesions that were stable for greater than 1000 seconds. As shown in Fig. 3F, the majority of both 1D and 3D adhesions (>65%) were maintained during this entire time period, whereas <20% of 2D FAs demonstrated such longevity. These data demonstrate that stabilized adhesions are intrinsic to 1D and 3D conditions versus 2D, which might play a prominent role in the more efficient cell migration in 1D and 3D.

Paxillin, vinculin, and actin demonstrate enhanced coupling within 1D adhesions

To explore further the possibility that increased adhesion stability in our 1D model is due to a fundamental change in individual protein associations within 1D and 2D adhesions, we analyzed adhesion protein kinetics by using fluorescence recovery after photobleaching (FRAP) in fibroblasts that expressed low levels of various adhesion proteins tagged with fluorescent proteins (Fig. 4A–E). Because FAs are thought to be structurally heterogeneous, with protein localization dependent on function (Kanchanawong et al., 2010), we compared proteins representing different functions within FAs; paxillin for signaling, vinculin for mechanotransduction, VASP for actin polymerization and actin for force generation.

We compared 1D adhesion and 2D FA assembly rates, focusing on the dynamics of adhesions that formed near the leading edge (≤2 µm from the membrane). Analysis of GFP–paxillin $t_{1/2}$ rates on 2D substrates, which represents its net incorporation into and movement out of a bleached region, agreed with a previous report (Fig. 4A,B) (von Wichert et al., 2003). By contrast, 1D adhesions demonstrated a twofold increase in turnover time, indicating a more stable association of paxillin in 1D adhesions (Fig. 4B,C). FRAP experiments with GFP–VASP showed a rapid turnover of VASP within 2D adhesions and, unlike paxillin, no differences were observed in 1D adhesions (Fig. 4D,E). Interestingly, in contrast to the localization of paxillin, vinculin and other previously described adhesion proteins (Doyle et al., 2009), VASP localized solely to the first 3 µm of 1D adhesions, with small amounts associating at the trailing edge. No VASP was detected beneath the cell body, in contrast to its known localization to FAs. Similar localization was also found for zyxin, a known VASP-binding partner (supplementary material Fig. S1A,B). These intriguing localization patterns suggest that the majority of actin polymerization occurs near the leading edge and is not locally affected by changing ECM topography.

To explore the mechanical aspects of 1D adhesions, we next focused on actin and vinculin. For a more direct visualization of protein dynamics, we used actin and vinculin constructs tagged with mKikGR, a photoconvertible fluorescent protein that changes from green emission to red after illumination with near ultraviolet (405 nm) light (Fig. 4F–J) (Habuchi et al., 2008).

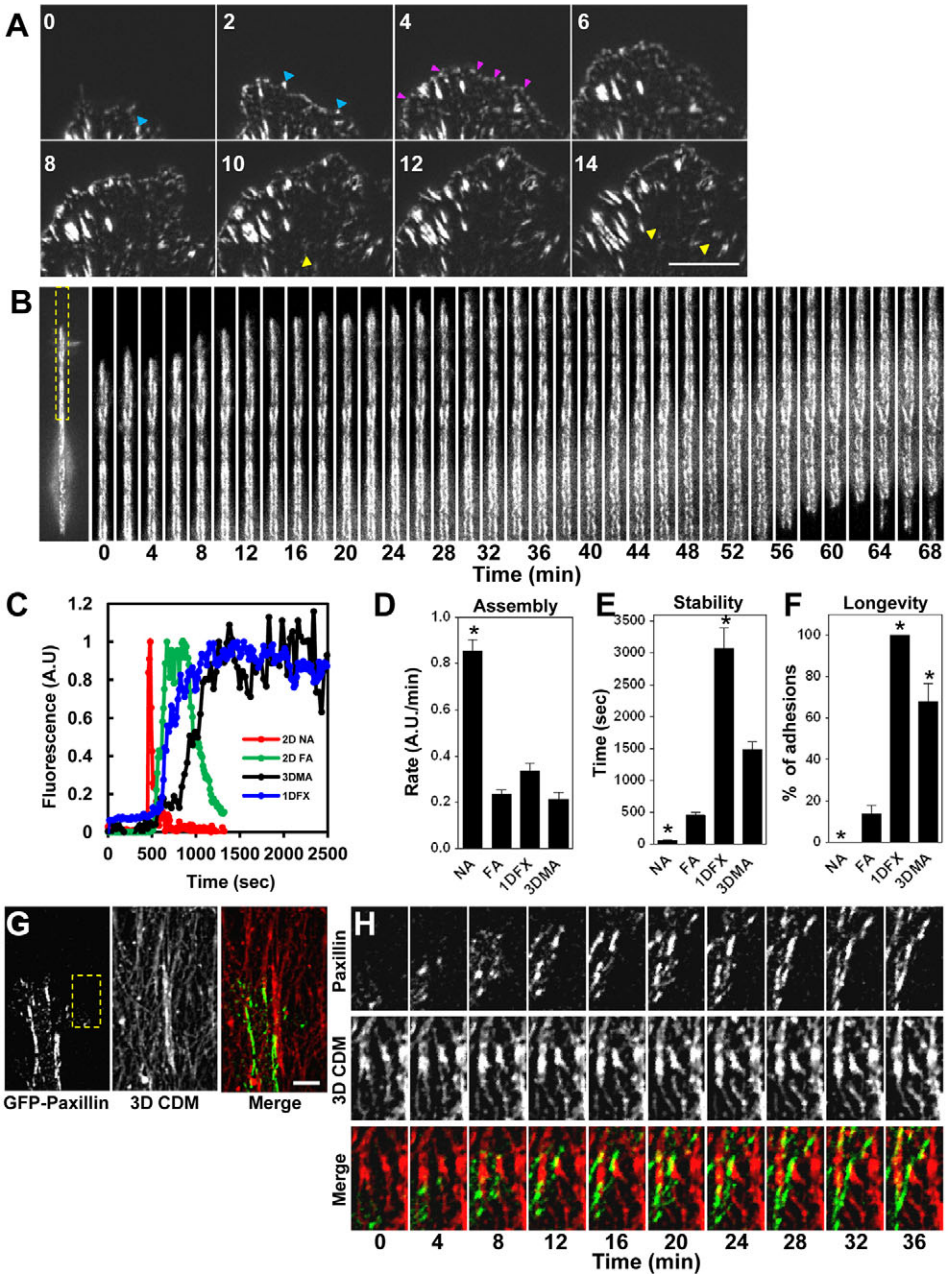

Fig. 3. Enhanced adhesion longevity of 1D and 3D matrix adhesions. (**A**) GFP–paxillin adhesions forming on 2D substrates involve small NAs (magenta triangles) and force-dependent FAs (blue triangles). Yellow triangles show adhesion disassembly of the FAs highlighted earlier. (**B**) 1D adhesions lack NAs and have a prolonged stability phase. (**C**) Examples of fluorescence changes over time, which illustrate the assembly and stability phases for NAs (red), FAs (green), 1D fibrillar adhesions (blue, 1DFXs) and 3D matrix adhesions (black, 3DMAs). (**D**) Assembly rates for NAs, FAs, 1DFXs and 3DMAs. (**E**) Average length of time of the stability phase for the four different adhesion types. (**F**) Percentage of adhesions with a stability phase longer than 1000 seconds. (**G**) GFP–paxillin-expressing NIH/3T3 fibroblast migrating through a 3D CDM. (**H**) Inset (yellow box in G) illustrates the stability of 3DMAs over an extended time. Scale bars: 10 μm.

Imaging of cells on 2D substrates using photoconverted mKikGR–vinculin confirmed that vinculin within FAs moves in a retrograde motion, with photoconverted molecules translocating from proximal to distal regions of a single adhesion (Fig. 4F). On a 2D surface, $t_{1/2}$ values for vinculin were longer than those for paxillin, which accords with other recent investigations (Wolfenson et al., 2011). Comparisons of data collected on 1D and 2D substrates revealed a twofold increase in vinculin $t_{1/2}$ rates, which were analogous to the paxillin $t_{1/2}$ rates analyzed by FRAP (Fig. 4G,H). Furthermore, velocity calculations showed a significant decrease in vinculin flow-rate within the 1D adhesions, indicating that a subpopulation of vinculin within 1D adhesions is more stably associated (Fig. 4J). It is possible that more vinculin molecules within 1D adhesions remain bound and stationary than in 2D FAs, suggesting increased coupling within 1D adhesions.

Because actin flow can vary greatly between the lamellipodia and lamellae of migrating cells, we photoconverted regions within the lamellipodia (0–2 μm from the membrane), and stress-fiber insertion points within an advancing lamella, for comparisons of 1D and 2D adhesions (Fig. 5). As expected, 2D lamellipodia (2D LA) showed rapid rearward actin flow with a short $t_{1/2}$, and high velocity of actin exiting from the photoconverted region (Fig. 5A). At stress-fiber insertion points (2D SF), actin movement slowed to <20% of 2D LA velocities, consistent with the binding of actin to FA components to reduce retrograde flow (Fig. 5B,C). Likewise, actin in cells on 1D substrates demonstrated reduced retrograde flow, as shown by the high $t_{1/2}$ and low velocity measurements (Fig. 5D–F). To discern how actin structures at the leading edge are formed in cells on 1D environments, we performed spinning-disk microscopy on cells stably expressing eGFP–actin (supplementary material Fig. S2). Rapid Z-series over time

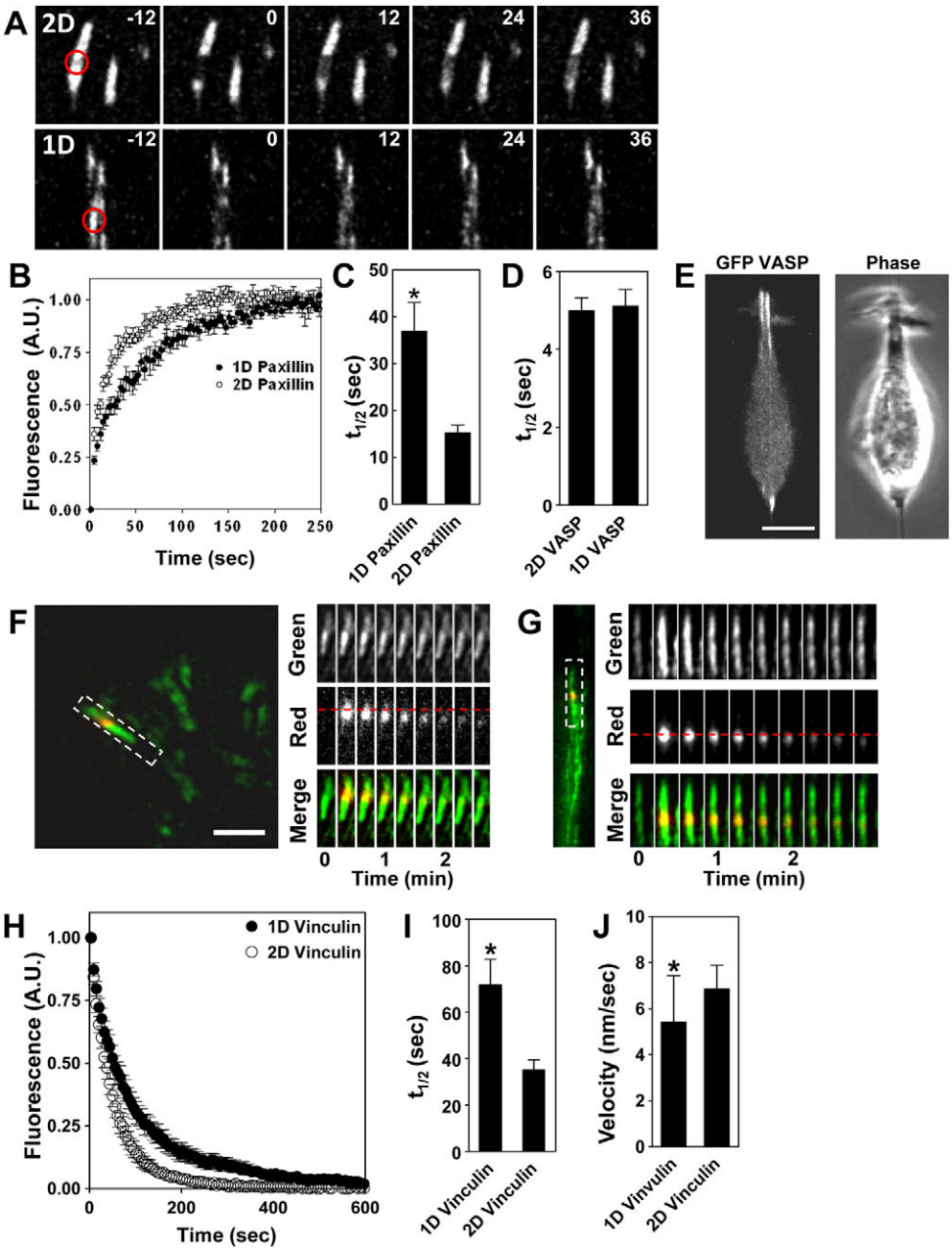

Fig. 4. 1D fibrillar adhesions show decreased adhesion turnover. (**A**) Comparison of 2D (upper) and 1D (lower) adhesions during FRAP analyses of GFP–paxillin. Red circles indicate the size of the FRAP region. (**B**,**C**) FRAP kinetic analyses of GFP–paxillin. (**D**) Analysis of GFP–VASP shows no difference in FRAP kinetics. (**E**) GFP–VASP localization (left) and a corresponding phase-contrast image of a NIH/3T3 fibroblast during 1D migration. (**F**,**G**) Photoconversion of mKikGR–vinculin within adhesions on 2D (F) and 1D (G) surfaces and changes over time. The box indicates the areas shown in the kymographs on the right. (**H**) mKikGR–vinculin average loss of fluorescence after photoconversion for 1D (black circles) and 2D (open circles) vinculin adhesions. (**I**) $t_{1/2}$ times for 1D and 2D vinculin adhesions. (**J**) Velocity measurements for vinculin within 1D and 2D adhesions. *P<0.05. Scale bars: E, 10 μm and F, 5 μm.

revealed that, unlike migration on 2D substrates, during 1D migration, lamellipodia rarely become associated with the ECM and instead extend upward and outward (supplementary material Fig. S2A,B). Furthermore, filopodia that might promote extension of the leading edge were observed (supplementary material Fig. S2C,D). Together, these results indicate that cell adhesions forming at the leading edge on 1D substrates are more stable, and that they have enhanced mechanical coupling through adhesion components, such as vinculin and paxillin.

Direct role of cell contractility in 1D migration efficiency through control of cell adhesions

Previous evidence suggests that reducing contractility alters the subtype of cell adhesions; focal and fibrillar adhesions disassemble whereas contractility-independent NAs are promoted (Vicente-Manzanares et al., 2007). Furthermore, blocking contractility with blebbistatin increases 2D cell-migration rates, yet loss of contractility has the opposite effect in both the 1D and 3D CDM, reducing cell-migration rates, suggesting a functional requirement when cells navigate through or on restricted ECM environments (Even-Ram et al., 2007; Doyle et al., 2009). Because of the previously established connection between 2D FA size and stability with cellular contractile force, we compared the dynamics of adhesions using mApple–paxillin in the presence of 25 μM blebbistatin. As expected, both fibrillar and focal adhesions were absent after the loss of physical force (Fig. 6A), because cells switched to using only force-independent NAs. Similar observations were made on 1D substrates, except that on a 2D surface, the majority of NAs formed at the leading edge (>60%), whereas adhesions on 1D substrates formed and disassembled in a fragmented, haphazard pattern along the entire length of the cell (Fig. 6B). Similar experiments performed in 3D CDM showed

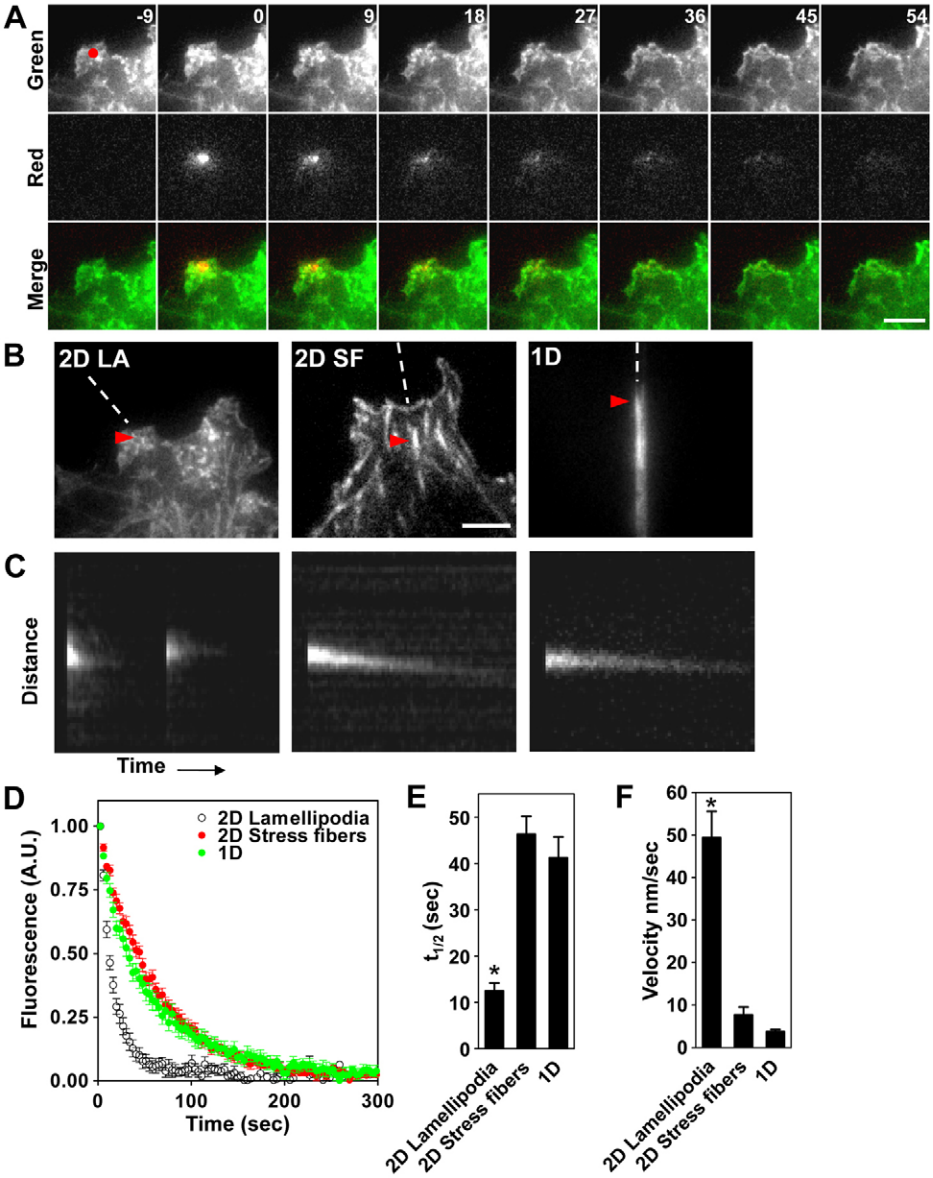

Fig. 5. Actin retrograde flow in 1D versus 2D conditions. (**A**) Photoconversion of mKikGR–actin within the lamellipodium of a migrating NIH/3T3 fibroblast showing the rapid kinetics within this region. The red dot indicates the photoconversion site. (**B**) Pre-conversion images showing 2D lamellipodial actin (2D LA), 2D stress fiber (2D SF) insertion points and the leading edge. The red arrowhead indicates the point of conversion, whereas the white dotted line illustrates the axis of the kymographs shown in C. (**C**) Kymographs of the photoconverted (red) sites shown in B. (**D**) mKikGR–actin average loss of fluorescence after photoconversion for 1D (green circles), 2D LA (open circles) and 2D SFs (red circles). (**E**) $t_{1/2}$ times for 1D, 2D LA and 2D SF actin. (**F**) Velocity measurements for actin within 1D, 2D FAs and 2D LA. *P<0.05. Scale bars: 5 μm.

comparable results (supplementary material Figs. S3,S4). Adhesions that were visible before treatment with blebbistatin decreased in size and became difficult to discern as cellular tension decreased, indicated by the relaxation of 3D CDM fibrils (supplementary material Fig. S3A,B, Movie 3). Immunostaining of blebbistatin-treated cells showed small, distinct paxillin-containing adhesions ~0.5–1 μm in diameter with fewer adhesions throughout the cell compared with untreated controls (supplementary material Fig. S4A,B). These data indicate that loss of contractility leads to reduced adhesion stability in all conditions.

Next, we analyzed integrin dynamics. To visualize activated β1 integrins, we added fluorescently labeled 9EG7 antibody at low concentrations (1.0 μg/ml) during live-cell TIRF imaging. Under control 2D conditions, 9EG7 was found along the leading edge and aggregated at sites of FAs (Fig. 6C). Distinct retrograde movement of integrins was observed as described previously (Pankov et al., 2000). Conversely, in the presence of blebbistatin, β1 integrin failed to accumulate in FA-like clusters and displayed no retrograde movement. That is, the β1 integrins remained stationary with respect to the underlying fibronectin matrix (Fig. 6D). Interestingly, integrins on 1D patterns showed no retrograde movement in control or blebbistatin conditions (Fig. 6E,F), suggesting greater engagement of integrins with the 1D ECM under control conditions. Together, these data suggest that loss of contractile force not only reduces adhesion longevity, but also results in a loss of coupling between integrins and adhesion components that is likely to be required for rapid migration on 1D patterns.

Differential regulation of myosin II isoforms A and B in adhesions and cell migration

Because blebbistatin induced loss of 1D adhesion stability, we determined which isoform of myosin II was responsible for the adhesion stabilization in 1D. The immuno-localization patterns of MIIA and MIIB (the two predominant isoforms) on 2D substrates was consistent with previous studies (Saitoh et al., 2001), with MIIA being more proximal to the leading edge than MIIB

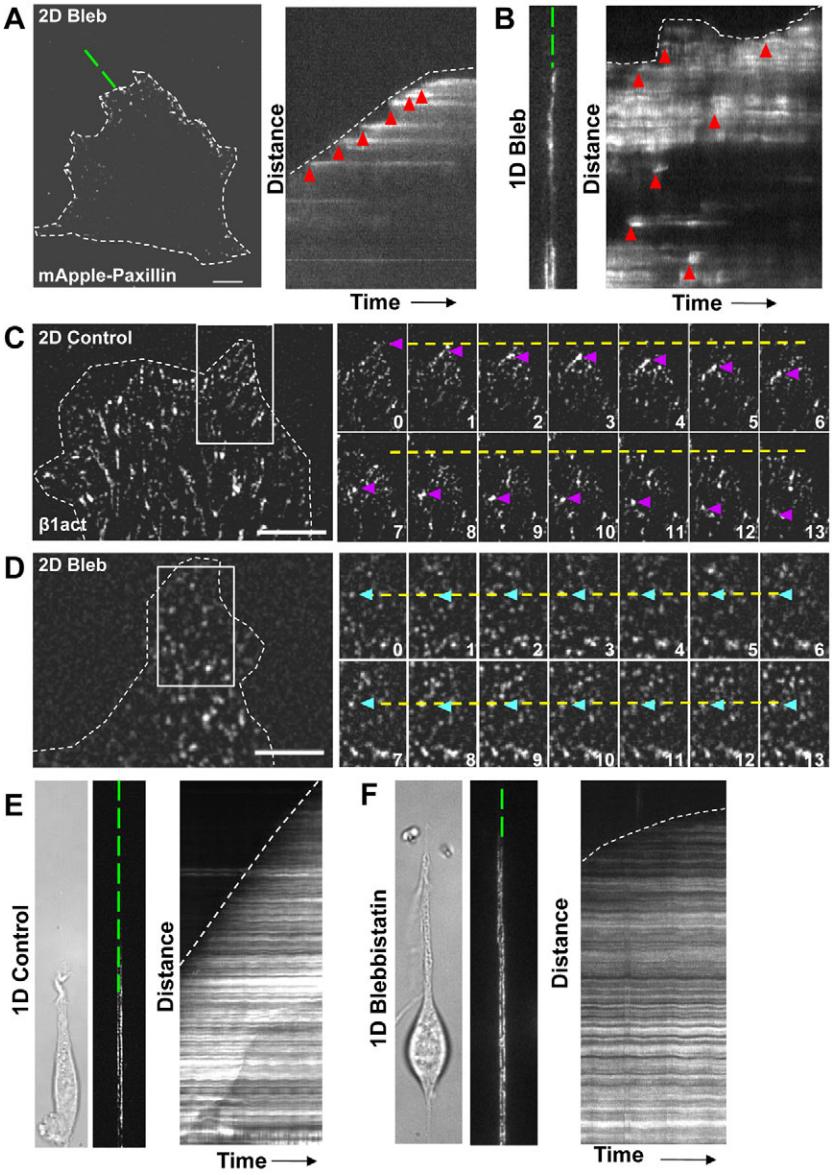

Fig. 6. Differential effects of loss of contractility. (**A**,**B**) Fibroblasts expressing mApple–paxillin show an altered distribution of adhesions on 2D (A) and 1D (B) surfaces after treatment with 25 μM blebbistatin. Kymographs illustrate the formation of NAs (red arrowheads) at the leading edge on 2D surfaces (A) and random formation on 1D surfaces (B). (**C**,**D**) Timelapse series showing AF568-labeled 9EG7 (activated β1 integrin) incorporation into adhesions on 2D surfaces in the control (C) or after treatment with 25 μM blebbistatin (D). Note the rearward movement of integrins in the control (purple arrowheads) and the lack of movement after treatment with blebbistatin (cyan arrowheads). The yellow dotted line indicates the original position of the adhesion. (**E**,**F**) Activated β1 integrin incorporation on 1D surfaces in the control (E) or after treatment with blebbistatin (F). Kymographs illustrate that integrins remain stationary and stable in either condition. The white dotted lines show the leading edge; the kymograph is shown at the green dotted line. Scale bars: 5 μm.

(MIIA:~1 μm, MIIB: >20 μm, supplementary material Fig. S5A,B). On 1D fibrillar lines, MIIA was also more proximal and was present ≤1 μm from the leading edge (supplementary material Fig. S5C), with MIIB being ≤ 5 μm from the leading edge.

We then used siRNA knockdown of either *MYH9* or *MYH10* (encoding MIIA and MIIB, respectively) in fibroblasts expressing GFP–paxillin to discern their relative contribution to adhesion stabilization. On 2D substrates, knockdown of *MYH9* resulted in the loss of FAs and formation of NAs, as previously described (Fig. 7A) (Vicente-Manzanares et al., 2007). Some FAs remained, primarily beneath the cell body associated with residual stress fibers (Fig. 7B; supplementary material Fig. S6A). On 1D fibrillar lines after knockdown of *MYH9*, the adhesions became transiently stable. That is, elongated adhesion structures remained under the length of the cell, but in a patchy distribution, and within the adhesions, paxillin was found to flux continuously rather than remaining stable (Fig. 7C–E; supplementary material Movie 4). Knockdown of *MYH9* mimicked blebbistatin treatment in decreasing the ability of cells to maintain leading-edge adhesions. Interestingly, even though knockdown of *MYH10* on 2D or 1D substrates did not generate substantial cell morphological changes (supplementary material Fig. S6B) or observable effects on the anterior portion of 1D adhesions, paxillin-containing adhesions underwent turnover at sites that were several microns behind the leading edge (Fig. 7F,G). These findings demonstrate a requirement for both MIIA and MIIB; MIIA is needed to reinforce adhesions at the leading edge after 1D ECM attachment, whereas MIIB stabilizes the remainder of the 1D adhesion during 1D migration.

Next, we determined the role of each isoform in migration efficiency. In our siRNA experiments, there were clear decreases in migration velocity after treatment with *MYH9* but not with *MYH10* siRNA. Because some of the cells did not show myosin II knockdown according to immunostaining, we turned to a conditional myosin II knockout system using primary mouse embryonic fibroblasts (MEFs) isolated from homozygous MIIA or MIIB floxed mice (Jacobelli et al., 2010; Ma et al., 2010). At

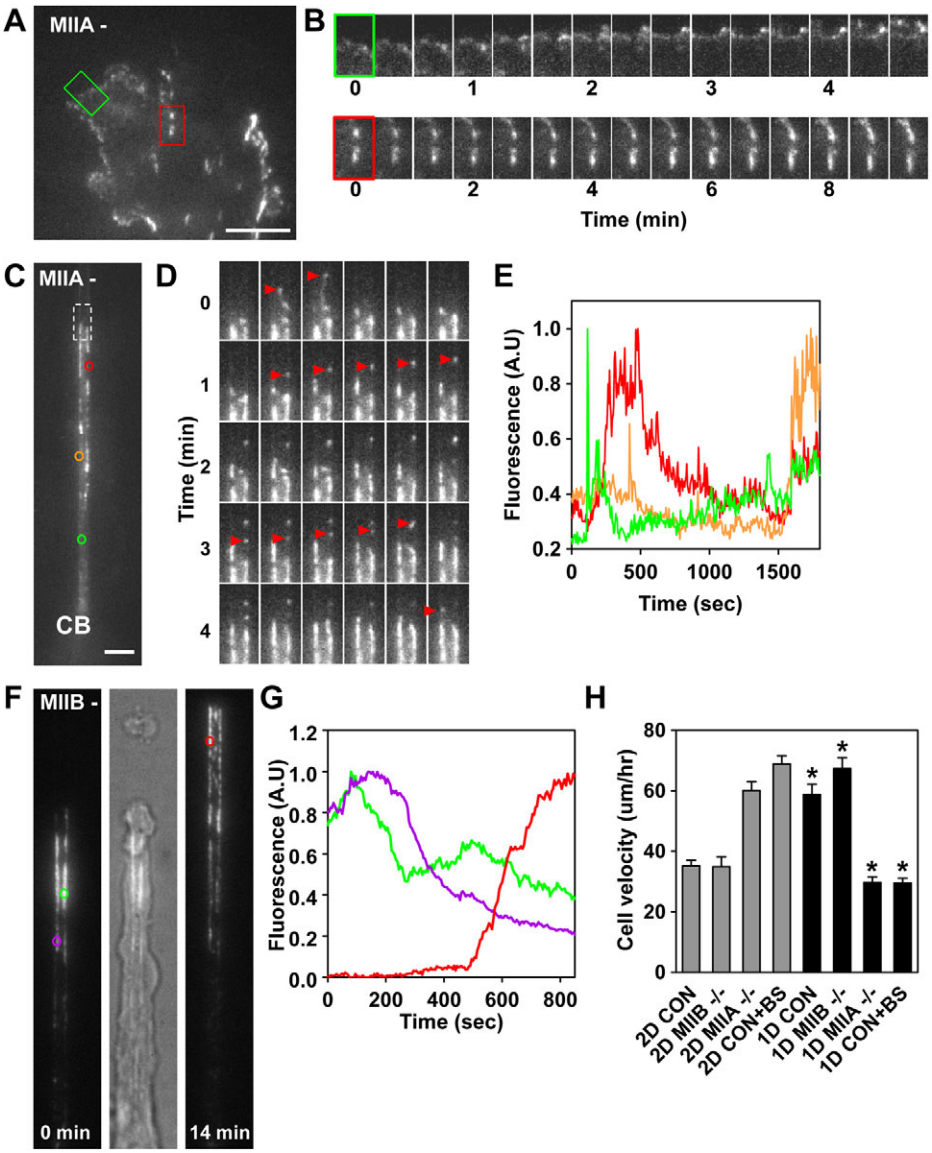

Fig. 7. Myosin II isoforms have different roles in cell adhesion and migration under 1D conditions. (**A**) SiRNA knockdown of *MYH9* results in the accumulation of NAs containing GFP–paxillin at the leading edge (green box) and central or posterior FAs (e.g. red box). (**B**) Time series for the insets in panel A comparing longevity of NAs (upper panel) and FAs (lower panel). (**C**) Remnants of 1D adhesions at various locations beneath the cell lose GFP–paxillin stability. (**D**) Time series (6 frames per minute) from the rectangle in panel C illustrates the instability of GFP–paxillin adhesion formation at the leading edge with nascent-like adhesions (red arrowheads). (**E**) Changes in fluorescence over time at the colored circles in panel C. (**F**) SiRNA knockdown of *MYH10* in fibroblasts expressing GFP–paxillin leads to adhesion turnover distal to the leading edge. GFP TIRF images and DIC are shown. Zero and 14-minute timepoints are presented to illustrate the change in adhesion turnover at different locations. (**G**) Changes in normalized fluorescence over time at the colored circles in panel F. (**H**) Ablation of the genes encoding either MIIA or MIIB reveals a differential requirement for MIIA in rapid 1D migration. Scale bars in A, B and C are 5, 2 and 2 μm, respectively. CB (C), cell body. $*P<0.05$.

96 hours after cells were treated with adenoviral GFP–Cre to delete the floxed exon, the cells showed a complete loss of either MIIA or MIIB protein depending on the targeted ablation (supplementary material Fig. S4); there were no compensatory effects on the levels of the other isoform, as shown previously (Jacobelli et al., 2010; Ma et al., 2010). Migration studies demonstrated that control adenoviral–GFP MEFs could migrate efficiently on 1D substrates, with a 1.7-fold higher velocity than on 2D surfaces (Fig. 7H). As expected, MIIA$^{-/-}$ MEFs on 2D substrates showed a morphology similar to that of cells treated with blebbistatin, and migrated more rapidly (1.7-fold increase compared with 2D controls), using broad lamellipodia at the front of well-spread cells. However, on 1D surfaces where lateral spreading was not possible, MIIA$^{-/-}$ MEF cells became more elongated (often ~500 μm in length, data not shown) and had inhibited rates of migration (Fig. 7H), similar to when control MEFs were treated with 25 μM blebbistatin.

Although Cre-mediated ablation of MIIB failed to alter migration speed in either 1D or 2D conditions compared with controls, MIIB$^{-/-}$ MEFs switched to an ‘inchworm’-like motion on 1D patterns. In summary, these data indicate that MIIA plays the main role in the adhesion-dependent contractility and adhesion maturation that is required for efficient 1D migration.

Loss of contractility reduces 1D protrusion efficiency

We investigated whether the changes in adhesion longevity and stability after loss of cellular contractility affected leading-edge dynamics under our 1D or 2D conditions, for example, by altered rates of cellular protrusion or P–R cycling. Within the first 10 minutes of treatment with 25 μM blebbistatin, fibroblasts in both 1D and 2D conditions displayed an initial burst of protrusive activity without a definitive retraction period. Subsequently, however, protrusiveness diverged markedly on 1D versus 2D surfaces (Fig. 8A,B). In 2D conditions, enhanced random cell protrusiveness continued at multiple cellular sites. By contrast, cells on 1D topographies demonstrated a reduced protrusion rate at the leading edge. Interestingly, lateral lamellipodial activity was observed perpendicular to the 1D fibrillar pattern in front of the main cell body, but not extending forwards; because the cells could not migrate laterally away from the lines, this protrusive

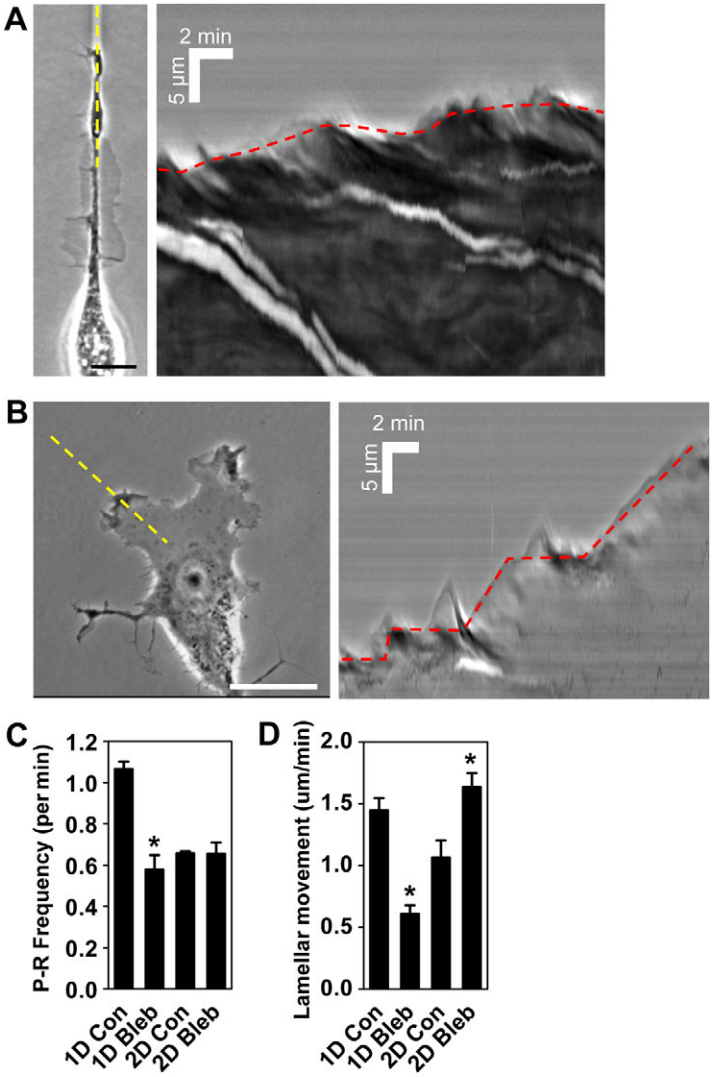

Fig. 8. Decreased contractility on 1D patterns results in loss of protrusion efficiency. (**A**,**B**) Analysis of protrusion dynamics in the presence of 25 μM blebbistatin on 1D (A) and 2D (B) substrates with the accompanying kymographs (from the yellow dotted line) on the right. The red dotted line in the kymograph indicates the lamellipodial–lamellar border. (**C**) Comparison of P–R frequency for both control and blebbistatin-treated cells. (**D**) Forwards movement of the lamella (red dotted line in A and B) for both control and blebbistatin-treated cells. *$P<0.05$ compared with dimensional control.

activity did not support cell migration (Fig. 8A). Analysis of leading-edge dynamics showed that the lack of contractile force reduced the 1D protrusion rate (threefold reduction: 3.8±4.4 versus 12.9±2.2), the frequency of the P–R cycle (Fig. 8C), and caused a significant reduction in protrusion distance (~27%). In contrast to these deficits, blebbistatin treatment on cells migrating on 2D substrates resulted in no significant alteration ($P>0.05$) in these parameters. It should be noted that in both conditions, the retraction distance was reduced (data not shown). The rate of lamellar advancement (calculated as the movement of the lamellipodial–lamellar border) was found to decrease in 1D conditions, whereas 2D conditions demonstrated a significant increase (Fig. 8D). These data indicate that in 1D conditions, force-dependent adhesions associated with the lamella provide a vital adhesion stabilization point that locally enhances leading-edge dynamics.

Discussion

In this study, we describe how the regulation of cell adhesion composition and dynamics through MII by different ECM topographies promotes efficient cell migration. We demonstrate that two key processes of mesenchymal cell migration, protrusion and adhesion are altered on 1D compared with 2D substrates. Protrusion is more efficient at the leading edge of cells on 1D substrates, as shown by increased lamellipodial extension and frequency, processes that are determined by the spatial organization of force-dependent adhesions within the lamella. Our data show that multiple components of cell adhesions, including paxillin, vinculin and actin are more stably associated within the 1D adhesion complex mediating adhesiveness to the underlying 1D ECM. This stabilization of components of the 'molecular clutch' involved in cell migration is dependent on the intracellular force generator MIIA. Together, these results establish that micro-environmental cues from topography can regulate cellular functions that include leading-edge protrusion and MII-dependent regulation of the composition, stability and function of cell adhesions in the process of rapid cell migration.

The ability of a cell to protrude efficiently involves many physical factors, including membrane tension, pushing forces from actin polymerization, retrograde flow of actin associated with MII contractility, traction forces exerted by FAs to the underlying matrix and frictional forces within focal adhesions. The latter forces, focused at the LP–LA border, act to counterbalance actin retrograde flow, which in turn allows

actin polymerization to produce leading edge protrusion (Choi et al., 2008). Recent biophysical modeling suggests that the force-dependent adhesions initiate the formation of the LP–LA border and its forwards progression (Shemesh et al., 2009). Frictional forces within FAs, the changing of focal adhesion size and their lateral distribution along the leading edge all contribute to lamellar movement and the slowing of actin retrograde flow. Here, we show that the oscillation frequency of the leading edge and the rates of protrusion are in fact dictated by simple alterations in ECM attachment through the lateral separation of adhesion plaques. On 2D dot matrices, the lamellipodia emanated only from points of ECM contact, suggesting that these sites of stability dictate the forwards progression of the lamella. By limiting lateral spreading and, hence, the separation of adhesions, a fibrillar topography increases protrusion frequency. Thus, local topographical features can regulate cellular protrusive processes.

Evidence from numerous studies indicates that MII-derived tension can greatly affect leading-edge dynamics. During cell spreading on 2D substrates, MII activity directly controls P–R cycles (Giannone et al., 2007). However, the main caveat surrounding this relationship is that the loss of contractility on 2D surfaces actually leads to an increase in the overall rate of cell migration. By contrast, why does migration in 3D and 1D environments require contractility? One main difference with regard to 2D migration involves the cellular adhesions. The adhesion stability and/or longevity shared by 1D and 3D adhesions compared with 2D NAs and FAs indicate that force-dependent stabilization of adhesions is an important factor for promoting migration in restricted environments. When contractility is inhibited, cells on 2D surfaces expand their leading edge to promote migration, which cannot occur in a restricted 1D or 3D fibrillar environment. This compensation is associated with the formation of numerous NAs at the leading edge that act together to promote lamellar movement. However, in a restricted environment, the lack of spreading reduces the number of adhesion sites that are available to aid in lamellar progression. Furthermore, our 3D imaging demonstrates that physical pulling of fibrils accompanies adhesion formation, and that loss of MII contraction results in both the loss of force that is applied to the fibrillar environment and adhesion stability.

Our results show that turnover rates for both vinculin and paxillin are reduced within 1D adhesions. That is, the individual proteins that normally fluctuate between FAs and the cytosol remain within adhesions for longer periods of time. Vinculin is associated with the generation of mechanical force (Grashoff et al., 2010), and its interactions with other proteins might be enhanced within 1D adhesions. Recently, other investigators have shown that the off-rates for vinculin, paxillin, and zxyin are greatly affected by contractile force, though in different ways (Wolfenson et al., 2011). Although vinculin and paxillin demonstrated substantial decreases in turnover within adhesions, neither VASP nor actin exhibited any alterations. In the case of VASP, one of its functions is to aid the polymerization of actin by limiting capping of free barbed-ends (Hansen and Mullins, 2010). The fact that there is no change in turnover indicates that the relative rate of actin polymerization is stable locally within adhesion sites. Together with the β1 integrin data, which demonstrates no slippage within 1D adhesions (unlike the results on 2D substrates), this suggests a greater integration of components between the integrins and the actin cytoskeleton. The apparent contradiction between this strong, prolonged 1D adhesive contact and rapid migration can be explained by efficient, tank-tread-like forwards advance of firmly adherent 1D adhesions.

The alterations in migration velocity on 1D and 2D surfaces in the absence of MIIA, even if opposite, underscore the important role that this isoform plays in mesenchymal cell force generation. This might be because of the high level of expression of MIIA compared with other isoforms (83%±7, MIIA; 17%±7, MIIB) (Ma et al., 2009). It has been shown previously that MII is required for migration in restricted environments wherein *Dictyostelium* migration is slowed in under-agarose cell migration assays (Laevsky and Knecht, 2003). Furthermore, T cells demonstrate different modes of migration after ablation of MIIA, suggesting that contractility plays a role, not only in the rate of migration, but also in the manner in which cells migrate (Jacobelli et al., 2009). If this idea is applied to fibroblast migration, it is conceivable that the large, broad lamellipodia, which are associated with a reduced contractile state in 2D that leads to enhanced migration, are not conducive to rapid migration on different physical structures such as fibrils. This concept is supported by the reduced leading-edge dynamics observed in the absence of contractility in our 1D model. Furthermore, the instability of adhesions at the leading edge after MIIA ablation suggests that MIIA is responsible for adhesion maturation. Overexpression of MIIA can increase the numbers and size of FAs near the leading edge, whereas MIIB cannot (Vicente-Manzanares et al., 2007). This suggests that MIIA is required for adhesion maturation, and without this vital function, cells in restricted environments cannot maintain adhesion integrity.

In summary, our findings provide new insights into how cellular interactions with fibrillar structures regulate cell migration. We show that efficient 1D cell migration requires MIIA-based contractility to increase adhesion stability and/or longevity at the leading edge, which is associated with enhanced protrusion dynamics. This association is likely to be the result of greater engagement of proteins that make up the molecular clutch.

Materials and Methods

Reagents

Sources were: rat anti-activated-β1 integrin 9EG7, rat anti-α5 integrin, and mouse anti-paxillin antibodies (BD Pharmingen); mouse anti-PY antibody (Upstate Biotechnology); rabbit anti-MIIA and rabbit anti-MIIB antibodies (Covance). Blebbistatin (–/–) (Calbiochem). Rabbit anti-fibronectin R745 antibody was generated in our laboratory.

Cell culture

NIH-3T3 fibroblasts (ATCC) were cultured in DMEM (Hyclone) containing 10% BCS (Hyclone), 100 U/ml penicillin-streptomycin (GIBCO) and 2 mM L-glutamine (GIBCO) at 37℃ in an atmosphere containing 10% CO_2. 3D matrices were prepared as described previously (Cukierman et al., 2001). MEFs were isolated at embryonic days 13.5 to 14.5 from homozygous mice and were genotyped using genomic DNA from the head and internal organs. MEFs were maintained at 37℃ in an atmosphere containing 5% CO_2 in DMEM supplemented with 10% FBS (Hyclone). All experiments were performed either on coverslips (Carolina Biological Supply Company, Burlington, NC) or MatTek dishes (MatTek, Ashland, MA), coated with 10 μg/ml fibronectin and blocked with BSA (MP Biomedicals, Solon, OH).

Plasmids, transfection and cell stablization

pmApple–paxillin and pmKIKGR were provided by Mike Davidson (Florida State University, Tallahassee, FL) and Atushi Miyawaki (Riken, Japan), respectively. pGFP-VASP and GFP–zyxin were provided by Jurgen Wehland (G and F National Research Center for Biotechnology, Germany). pGFP-paxillin and pGFP-vinculin were described previously (Doyle et al., 2009). mKikGR flanked by *Nhe*I and *Bgl*II was amplified by PCR from pRSETb mKikGR and inserted into *Nhe*I and *Bgl*II sites of pEGFP NBC1 to construct pmKikGR. Human β-actin was excised from

pmCherry-actin with *Bam*HI and *Xba*I. The actin fragment was inserted into the *Bam*HI and *Xba*I site of the pmKikGR NBC1 to construct pmKikGR actin. pmKIKGR-vinculin was subcloned from pEGFP-vinculin using *Hind*III and *Xba*I. pmCherry-N1 was provided by Erik Snapp (Albert Einstein College of Medicine, NY). pmCherry-zyxin was constructed by excision from pGFP-zyxin with *Bam*H1 and *Eco*RI, and insertion into the *Bam*HI-*Eco*RI site of pmCherry-N1. Each construct was verified by sequencing. Plasmids were transfected into NIH-3T3 fibroblasts by electroporation using a Bio-Rad Gene Pulsar TM at 170V, 960 μFd with external capacitance and a time constant of 17–22 μs in 0.4 cm gap cuvettes. Most transfected cells were selected using 300 IU/ml of geneticin (GIBCO) for two weeks before being sorted for fluorescence using a Beckman Coulter MoFlo Legacy Cell Sorter (Fullerton, CA).

Adenoviral growth and MEF infection

Adenoviral GFP–Cre was a generous gift from Hillary Beggs (The University of California, San Francisco, CA), and control adenoviral GFP was from Clontech. For infection, MEFs were plated at 4×10^5 cells in a 100 mm dish and grown overnight, then treated with 50 μl of either the GFP control or GFP–Cre virus (titer of 9.36×10^{11}) in 4 ml supplemented DMEM for 1 hour, followed by another 4 ml, and were then incubated overnight. Cells were rinsed and re-plated into new dishes, and were used 96 hours after infection for up to two passages.

siRNA

MYH9 and *MYH10* siRNAs were obtained as SMARTpool plus preparations and single duplexes (Dharmacon, Lafayette, CO). siRNA transfections were performed as described previously (Pankov et al., 2005).

Immunofluorescence staining

All fixation and permeablization steps were performed at 37℃. Cells were permeabilized and fixed in 1% paraformaldehyde and 0.03% Triton X-100 with 10 μg/ml nonfluorescent phalloidin (Invitrogen) in cytoskeletal buffer (CBS; 10 mM MES, 138 mM KCl, 2 mM EGTA, 3 mM $MgCl_2$ plus 5% sucrose, pH 6.9) for 90 seconds and postfixed in 4% paraformaldehyde in CBS for 15 minutes. Cells were rinsed three times in PBS^{++} and permeabilized with 0.5% Triton X-100 in CBS for 5 minutes. Cells were rinsed three times over 20 minutes with PHEM plus glycine (60 mM PIPES, 2 mM HEPES, 10 mM EGTA, 2 mM $MgCl_2$, 100 mM glycine, pH 6.9). Non-specific sites were blocked with 20% donkey serum (Jackson ImmunoResearch Laboratories), together with M.O.M. reagent (Vector Laboratories) in PHEM plus glycine buffer for 1 hour. Cells were rinsed three times with PHEM plus glycine for 30 minutes. Both primary and secondary antibodies were diluted in PHEM plus glycine with 10% donkey serum and incubated for 25 minutes. Secondary antibodies were from Jackson ImmunoResearch Laboratories.

MicroPhotoablation

Microphotoablation was performed as detailed elsewhere (Doyle, 2009).

Confocal microscopy

Confocal microscopy images were obtained using an LSM 510 NLO META confocal microscope equipped with A-Plan-Apochromat 63× [numerical aperture (NA) 1.4] (Zeiss, Thornwood, NY). 488 nm argon, 543 nm HeNe1 and 633 nm HeNe2 lasers were used to excite Cy2, Cy3 and Cy5 fluorophores, respectively. The pinholes for each laser line were aligned for optimal confocality. Alternatively, a Zeiss 710 LSM confocal system was used with a similar laser setup.

Live-cell 3D imaging

For 3D CDM and for imaging requiring Z-stacks of live GFP-expressing fibroblasts, we used a CSU-X1 spinning disk (Yokogawa, Tokyo, Japan) attached to a Zeiss Axiovert 200M microscope using a 100× Plan-ApoChromat oil-immersion objective (NA, 1.4). An LMM5 (Spectral Applied Research, Ontario, Canada) equipped with 405 nm (100 mW), 488 nm (100 mW), 561 (50 mW) and 642 nm (100 mW) diode lasers was used for excitation. The primary dichroic (405/488/561/640) and accompanying emission filters were from Semrock (Rochester, NY). Images were captured using a Hamamatsu 512 back-thinned EM CCD camera. An objective-based piezo stage (Prior Scientific, Cambridge, UK) was used to capture Z-stacks. An environmental chamber on the microscope maintained a constant temperature of 37℃, and constant CO_2 and humidity. All components were controlled with MetaMorph imaging software (Molecular Devices, Downington, PA).

TIRF Microscopy

Multi-color TIRF imaging was performed using an Olympus IX-71 microscope equipped with three TIRF illuminator arms using a TIRFM UIS2 UApo 150× (NA, 1.45) objective. Excitation was provided by single fiber-coupled diode lasers. The 488 nm (33 mW) and 561 nm (33 mW) lasers were from Point Source (Mitchell Point, Hamble, UK) and the 405 nm (30 mW) laser was from Coherent (Santa Clara, CA, USA). All TIRF illuminators were aligned properly for each laser wavelength. Single emission filters (520, 605 and 690) and triple dichroic (488/568/647) mirrors were from Chroma or Semrock (405/488/561). Images were captured using a Cascade II:1024B EM CCD camera (Photometrics, Tucson, AZ). A Lambda 10-4 filterwheel was used with single emission filters. All hardware was controlled through MetaMorph. A custom environmental chamber (Precision Plastics, Beltsville, MD) maintained cells at 37℃ with 10% CO_2. Images of cells were captured every 2.5–10 seconds depending on the experiment, using ~5% laser light. All images of cells were captured in the presence of Oxyfluor (Oxyrase, Mansfield, OH) to minimize photobleaching and phototoxicity.

Photoconversion experiments

For the photoconversion of mKiKgr–actin or vinculin, images of cells were captured every 2.5–5 seconds, and in every frame for green (488 excitation) and red (561 excitation) channels. A 50 micron pinhole (CVI Melles Griot, Carlsbad, CA) was fitted into the field diaphragm position of the 405 nm diode TIRF illuminator arm and focused to the back focal plane of the objective. A MetaMorph journal was created to trigger a 1 second 405 nm laser pulse at 100% power.

FRAP and photoconversion analysis

FRAP data were collected on a Zeiss LSM 510 NLO system using a 63× Plan-ApoChromat oil-immersion objective (NA, 1.3). The FRAP area was a 1.48 μm^2 region at the middle of the adhesion. FRAP kinetics were analyzed in a similar manner to Humphries and colleagues (Humphries et al., 2007). Briefly, each FRAP time series was adjusted for photobleaching using ImageJ software (NIH, Bethesda, MD). To calculate $t_{1/2}$ times, fractional fluorescence was plotted based on calculations from Snapp and colleagues ($F2(T)=[F(t)-F0]/[F_\infty-F0]$) (Snapp et al., 2003). For analysis of mKIKGR experiments, fractional fluorescence was plotted again, except that the asymptote (F_∞) was exchanged for maximum fluorescence (Fm) after conversion, and the immediate post-bleach ROI measurement ($F0$) was exchanged for a pre-bleach background (Fbg) ($F2(T)=[F(t)-Fbg]/[Fm-Fbg]$). Both data sets were then fit with single exponential recovery curves for calculating $t_{1/2}$ values.

Timelapse imaging

Timelapse movies were recorded on a Zeiss Axiovert 135TV as described previously (Doyle et al., 2009).

Image Processing

Image processing was carried out using custom-made smoothing, sharpening and convolution filters using MetaMorph software. For cells whose images were captured in a 3D cell-derived matrix, Z-stacks of each wavelength were either averaged or summed together to generate Z-projected or 2D images. Filter kernel settings and other processing steps will be provided on request.

Statistics

Prism 4 by GraphPad software was used for all graphs and statistical analysis. One-way ANOVA, using a Tukey post-test for more than two data sets, and Mann-Whitney t-tests, were used to establish significant differences ($P<0.05$). All error bars indicate the standard error of the mean.

Acknowledgements

We thank J. Harunaga, R. Petrie, E. Joo and T. Laemmermann for stimulating discussions and helpful suggestions.

Funding

Supported by the Intramural Research Program of the National Institute of Dental and Craniofacial Research, National Institutes of Health [project numbers DE000524 and DE000718]. Deposited in PMC for release after 12 months.

Supplementary material available online at
http://jcs.biologists.org/lookup/suppl/doi:10.1242/jcs.098806/-/DC1

References

Burnette, D. T., Manley, S., Sengupta, P., Sougrat, R., Davidson, M. W., Kachar, B. and Lippincott-Schwartz, J. (2011). A role for actin arcs in the leading-edge advance of migrating cells. *Nat. Cell Biol.* **13**, 371-382.

Choi, C. K., Vicente-Manzanares, M., Zareno, J., Whitmore, L. A., Mogilner, A. and Horwitz, A. R. (2008). Actin and alpha-actinin orchestrate the assembly and maturation of nascent adhesions in a myosin II motor-independent manner. *Nat. Cell Biol.* **10**, 1039-1050.

Cukierman, E., Pankov, R., Stevens, D. R. and Yamada, K. M. (2001). Taking cell-matrix adhesions to the third dimension. *Science* **294**, 1708-1712.

Doyle, A. D. (2009). Generation of micropatterned substrates using micro photopatterning. *Curr. Protoc. Cell Biol.* **Chapter 10**, Unit 10 15.

Doyle, A. D., Wang, F. W., Matsumoto, K. and Yamada, K. M. (2009). One-dimensional topography underlies three-dimensional fibrillar cell migration. *J. Cell Biol.* **184**, 481-490.

Even-Ram, S., Doyle, A. D., Conti, M. A., Matsumoto, K., Adelstein, R. S. and Yamada, K. M. (2007). Myosin IIA regulates cell motility and actomyosin-microtubule crosstalk. *Nat. Cell Biol.* **9**, 299-309.

Friedl, P. and Wolf, K. (2010). Plasticity of cell migration: a multiscale tuning model. *J. Cell Biol.* **188**, 11-19.

Giannone, G., Dubin-Thaler, B. J., Rossier, O., Cai, Y., Chaga, O., Jiang, G., Beaver, W., Döbereiner, H. G., Freund, Y., Borisy, G. et al. (2007). Lamellipodial actin mechanically links myosin activity with adhesion-site formation. *Cell* **128**, 561-575.

Grashoff, C., Hoffman, B. D., Brenner, M. D., Zhou, R., Parsons, M., Yang, M. T., McLean, M. A., Sligar, S. G., Chen, C. S., Ha, T. et al. (2010). Measuring mechanical tension across vinculin reveals regulation of focal adhesion dynamics. *Nature* **466**, 263-266.

Gupton, S. L. and Waterman-Storer, C. M. (2006). Spatiotemporal feedback between actomyosin and focal-adhesion systems optimizes rapid cell migration. *Cell* **125**, 1361-1374.

Habuchi, S., Tsutsui, H., Kochaniak, A. B., Miyawaki, A. and van Oijen, A. M. (2008). mKikGR, a monomeric photoswitchable fluorescent protein. *PLoS ONE* **3**, e3944.

Hansen, S. D. and Mullins, R. D. (2010). VASP is a processive actin polymerase that requires monomeric actin for barbed end association. *J. Cell Biol.* **191**, 571-584.

Hu, K., Ji, L., Applegate, K. T., Danuser, G. and Waterman-Storer, C. M. (2007). Differential transmission of actin motion within focal adhesions. *Science* **315**, 111-115.

Humphries, J. D., Wang, P., Streuli, C., Geiger, B., Humphries, M. J. and Ballestrem, C. (2007). Vinculin controls focal adhesion formation by direct interactions with talin and actin. *J. Cell Biol.* **179**, 1043-1057.

Jacobelli, J., Bennett, F. C., Pandurangi, P., Tooley, A. J. and Krummel, M. F. (2009). Myosin-IIA and ICAM-1 regulate the interchange between two distinct modes of T cell migration. *J. Immunol.* **182**, 2041-2050.

Jacobelli, J., Friedman, R. S., Conti, M. A., Lennon-Dumenil, A. M., Piel, M., Sorensen, C. M., Adelstein, R. S. and Krummel, M. F. (2010). Confinement-optimized three-dimensional T cell amoeboid motility is modulated via myosin IIA-regulated adhesions. *Nat. Immunol.* **11**, 953-961.

Kanchanawong, P., Shtengel, G., Pasapera, A. M., Ramko, E. B., Davidson, M. W., Hess, H. F. and Waterman, C. M. (2010). Nanoscale architecture of integrin-based cell adhesions. *Nature* **468**, 580-584.

Kiuchi, T., Ohashi, K., Kurita, S. and Mizuno, K. (2007). Cofilin promotes stimulus-induced lamellipodium formation by generating an abundant supply of actin monomers. *J. Cell Biol.* **177**, 465-476.

Laevsky, G. and Knecht, D. A. (2003). Cross-linking of actin filaments by myosin II is a major contributor to cortical integrity and cell motility in restrictive environments. *J. Cell Sci.* **116**, 3761-3770.

Ma, X., Takeda, K., Singh, A., Yu, Z. X., Zerfas, P., Blount, A., Liu, C., Towbin, J. A., Schneider, M. D., Adelstein, R. S. et al. (2009). Conditional ablation of nonmuscle myosin II-B delineates heart defects in adult mice. *Circ. Res.* **105**, 1102-1109.

Ma, X., Jana, S. S., Conti, M. A., Kawamoto, S., Claycomb, W. C. and Adelstein, R. S. (2010). Ablation of nonmuscle myosin II-B and II-C reveals a role for nonmuscle myosin II in cardiac myocyte karyokinesis. *Mol. Biol. Cell* **21**, 3952-3962.

Pankov, R., Cukierman, E., Katz, B. Z., Matsumoto, K., Lin, D. C., Lin, S., Hahn, C. and Yamada, K. M. (2000). Integrin dynamics and matrix assembly: tensin-dependent translocation of alpha(5)beta(1) integrins promotes early fibronectin fibrillogenesis. *J. Cell Biol.* **148**, 1075-1090.

Pankov, R., Endo, Y., Even-Ram, S., Araki, M., Clark, K., Cukierman, E., Matsumoto, K. and Yamada, K. M. (2005). A Rac switch regulates random versus directionally persistent cell migration. *J. Cell Biol.* **170**, 793-802.

Parsons, J. T., Horwitz, A. R. and Schwartz, M. A. (2010). Cell adhesion: integrating cytoskeletal dynamics and cellular tension. *Nat. Rev. Mol. Cell Biol.* **11**, 633-643.

Pasapera, A. M., Schneider, I. C., Rericha, E., Schlaepfer, D. D. and Waterman, C. M. (2010). Myosin II activity regulates vinculin recruitment to focal adhesions through FAK-mediated paxillin phosphorylation. *J. Cell Biol.* **188**, 877-890.

Petrie, R. J., Doyle, A. D. and Yamada, K. M. (2009). Random versus directionally persistent cell migration. *Nat. Rev. Mol. Cell Biol.* **10**, 538-549.

Provenzano, P. P. and Keely, P. J. (2009). The role of focal adhesion kinase in tumor initiation and progression. *Cell Adhes. Migr.* **3**, 347-350.

Ridley, A. J. (2011). Life at the leading edge. *Cell* **145**, 1012-1022.

Ridley, A. J., Schwartz, M. A., Burridge, K., Firtel, R. A., Ginsberg, M. H., Borisy, G., Parsons, J. T. and Horwitz, A. R. (2003). Cell migration: integrating signals from front to back. *Science* **302**, 1704-1709.

Saitoh, T., Takemura, S., Ueda, K., Hosoya, H., Nagayama, M., Haga, H., Kawabata, K., Yamagishi, A. and Takahashi, M. (2001). Differential localization of non-muscle myosin II isoforms and phosphorylated regulatory light chains in human MRC-5 fibroblasts. *FEBS Lett.* **509**, 365-369.

Shemesh, T., Verkhovsky, A. B., Svitkina, T. M., Bershadsky, A. D. and Kozlov, M. M. (2009). Role of focal adhesions and mechanical stresses in the formation and progression of the lamellipodium-lamellum interface. *Biophys. J.* **97**, 1254-1264.

Snapp, E. L., Altan, N. and Lippincott-Schwartz, J. (2003). Measuring protein mobility by photobleaching GFP chimeras in living cells. *Curr. Protoc. Cell Biol.* **Chapter 21**, Unit 21 21.

Vicente-Manzanares, M., Zareno, J., Whitmore, L., Choi, C. K. and Horwitz, A. F. (2007). Regulation of protrusion, adhesion dynamics, and polarity by myosins IIA and IIB in migrating cells. *J. Cell Biol.* **176**, 573-580.

von Wichert, G., Haimovich, B., Feng, G. S. and Sheetz, M. P. (2003). Force-dependent integrin-cytoskeleton linkage formation requires downregulation of focal complex dynamics by Shp2. *EMBO J.* **22**, 5023-5035.

Wolfenson, H., Bershadsky, A., Henis, Y. I. and Geiger, B. (2011). Actomyosin-generated tension controls the molecular kinetics of focal adhesions. *J. Cell Sci.* **124**, 1425-1432.